



University of Pennsylvania
ScholarlyCommons

Department of Physics Papers

Department of Physics

5-30-2008

Order Parameters and Phase Diagram of Multiferroic $R\text{Mn}_2\text{O}_5$

A. Brooks Harris

University of Pennsylvania, harris@dept.physics.upenn.edu

Amnon Aharony

Ben Gurion University

Ora Entin-Wohlman

Ben Gurion University

Follow this and additional works at: http://repository.upenn.edu/physics_papers

 Part of the [Physics Commons](#)

Recommended Citation

Harris, A. B., Aharony, A., & Entin-Wohlman, O. (2008). Order Parameters and Phase Diagram of Multiferroic $R\text{Mn}_2\text{O}_5$. Retrieved from http://repository.upenn.edu/physics_papers/102

Suggested Citation:

A.B. Harris, A. Aharony and O. Entin-Wohlman. (2008). "Order Parameters and Phase Diagram of Multiferroic $R\text{Mn}_2\text{O}_5$." *Physical Review Letters*. **100**, 217202.

© 2008 The American Physical Society

<http://dx.doi.org/10.1103/PhysRevLett.100.217202>

This paper is posted at ScholarlyCommons. http://repository.upenn.edu/physics_papers/102

For more information, please contact repository@pobox.upenn.edu.

Order Parameters and Phase Diagram of Multiferroic RMn_2O_5

Abstract

The generic magnetic phase diagram of multiferroic RMn_2O_5 (with $R = Y, Ho, Tb, Er, Tm$), which allows different sequences of ordered magnetic structures for different R 's and different control parameters, is described using order parameters which explicitly incorporate the magnetic symmetry. A phenomenological magnetoelectric coupling is used to explain why some of these magnetic phases are also ferroelectric. Several new experiments, which can test this theory, are proposed.

Disciplines

Physical Sciences and Mathematics | Physics

Comments

Suggested Citation:

A.B. Harris, A. Aharony and O. Entin-Wohlman. (2008). "Order Parameters and Phase Diagram of Multiferroic RMn_2O_5 ." *Physical Review Letters*. **100**, 217202.

© 2008 The American Physical Society

<http://dx.doi.org/10.1103/PhysRevLett.100.217202>

Order Parameters and Phase Diagram of Multiferroic RMn_2O_5

A. B. Harris,¹ Amnon Aharony,^{2,*} and Ora Entin-Wohlman^{2,*}

¹Department of Physics and Astronomy, University of Pennsylvania, Philadelphia, Pennsylvania 19104, USA

²Department of Physics, Ben Gurion University, Beer Sheva 84105, Israel

(Received 11 February 2008; published 30 May 2008)

The generic magnetic phase diagram of multiferroic RMn_2O_5 (with $R = Y, Ho, Tb, Er, Tm$), which allows different sequences of ordered magnetic structures for different R 's and different control parameters, is described using order parameters which explicitly incorporate the magnetic symmetry. A phenomenological magnetoelectric coupling is used to explain why some of these magnetic phases are also ferroelectric. Several new experiments, which can test this theory, are proposed.

DOI: 10.1103/PhysRevLett.100.217202

PACS numbers: 75.25.+z, 75.10.Jm, 75.40.Gb

There has recently been much interest in multiferroics, which display simultaneous magnetic and ferroelectric (FE) ordering [1–4]. In particular, the orthorhombic family RMn_2O_5 (RMO), where R is a rare earth, exhibits interesting sequences of magnetic density wave orderings, with varying wave vector \mathbf{q} , and some of these phases are also FE [2,5–9]. In all these phases one has $q_y = 0$, while $|q_x - \frac{1}{2}| \lesssim 0.02$ and $|q_z - \frac{1}{4}| \lesssim 0.02$. Cooling from the paramagnetic (PM) phase, one first enters a phase in which both q_x and q_z are incommensurate. We call this phase Π_1 ($I =$ “incommensurate”, and the subscript will be explained below; some experimental papers call this phase 2DIC). For $R = Y$ [5], Er [6] and Tm [8], further cooling yields transitions into a phase which we call IC_2 (also called 1DIC), where q_x is still incommensurate, while $q_z = \frac{1}{4}$ ($C =$ “commensurate”), then into a “CC” phase (also called CM), with $\mathbf{q} = (\frac{1}{2}, 0, \frac{1}{4})$, and finally into a phase where both q_x and q_z are incommensurate again (“ Π_2 ”, or LTI-2DIC). $R = Ho$ [9] and Tb [7] go directly from Π_2 to CC. For $R = Er$, the low temperature (T) phase has $q_x = \frac{1}{2}$, while q_z is incommensurate (“CI”, or LTI-1DIC). While the phases IC_2 and CC exhibit a FE moment \mathbf{P} along the $y(b)$ axis, such a moment appears in only some of the observed low T phases [10,11]. Up to now, the microscopic theories of these systems are controversial, and a phenomenological description which provides a unified explanation of this complicated phase behavior does not exist. The present Letter rectifies this situation, and provides a basis for analyses of other multiferroics with large unit cells.

Although group theory has been applied to neutron diffraction data from magnetic materials [12], its implications for multiferroics have not been fully exploited until the definitive analyses of $Ni_3V_2O_8$ and $TbMnO_3$ [3,4,13–15]. Following the same approach, we identify the order parameters (OP's) allowed by symmetry [16] and find the generic phase diagram for RMO systems (Fig. 1), which allows for the observed sequences of phases. The theory also explains (a) which phases are simultaneously magnetic and ferroelectric, (b) the occurrence of two distinct spin structures in neutron diffraction studies of the CC

phase [5,17], and makes several new predictions, which can be tested experimentally.

The PM unit cell of the RMO's contains 4 Mn^{3+} , 4 Mn^{4+} and 4 R^{3+} ions. Denoting these ions by $\tau (= 1, \dots, 12)$, and the corresponding Fourier transforms of the α -spin-components by $S_\alpha(\mathbf{q}, \tau)$, the quadratic terms in the Landau free energy F_M are

$$F_{M,2} = \frac{1}{2} \sum_{\mathbf{q}, \alpha, \beta; \tau, \tau'} \chi_{\alpha\beta}^{-1}(\mathbf{q}; \tau, \tau') S_\alpha(\mathbf{q}, \tau) S_\beta(\mathbf{q}, \tau'). \quad (1)$$

In principle one would diagonalize the (36×36) inverse susceptibility matrix $\chi_{\alpha\beta}^{-1}(\mathbf{q}; \tau, \tau')$ (determined by the various magnetic interactions). As T is lowered, the first phase to order corresponds to the eigenvalue which approaches zero first. The degeneracy of this eigenvalue has two origins: first, all the n_q wave vectors in the star of symmetry-related optimal wave vectors \mathbf{q} 's have the same eigenvalue. Second, each of these \mathbf{q} 's is associated with irreducible representations (irrep's) Γ of the PM symmetry group of \mathbf{q} (the “little group”) [18]. Excepting accidental degeneracy, a continuous transition from the PM phase involves only a single irrep. If this critical irrep is d

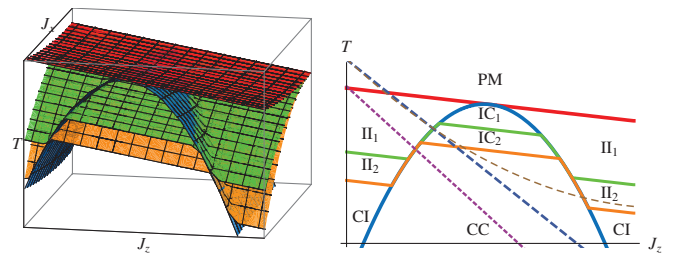


FIG. 1 (color). Left-hand side (LHS): Schematic 3D phase diagram for q_x (q_z) near $\frac{1}{2}$ ($\frac{1}{4}$). J_x and J_z are parameters which control q_x and q_z . The red surface separates PM and Π_1 . Below the blue surface one has $q_z = \frac{1}{4}$, in phases IC_1 and IC_2 . The green surfaces represent $\Pi_1 \rightarrow \Pi_2$ and $IC_1 \rightarrow IC_2$. Below the orange surfaces $q_x = \frac{1}{2}$, in phases CI or CC. RHS: a cut at constant $q_x \neq 1/2$. The dashed and dotted lines represent proposed trajectories for specific RMO's, as T is varied.

dimensional (dD), then this eigenvalue is dn_q -fold degenerate and this manifold is described by dn_q real OP's, or $dn_q/2$ complex ones. Each complex OP represents the amplitude and the phase of the spin ordering eigenfunction, $\{S_\alpha(\mathbf{q}, \tau)\}$. The symmetry of the eigenfunction is associated with the irrep and is inherited by the OP's.

For each RMO, the optimal wave vector \mathbf{q} is determined by its specific material (e.g. the exchange and anisotropy energies) and experimental (e.g., pressure, magnetic field) parameters. We represent these control parameters by their combinations, denoted J_x and J_z , which fix the values of q_x and q_z , respectively. Figure 1 shows the phase diagram of the RMO's in terms of J_x and J_z . Following experiments, we fix $q_y = 0$. We start with the case $q_x \neq \frac{1}{2}$ (with q_z near $\frac{1}{4}$). For each such \mathbf{q} , the "little" group contains only unity and m_y , which maps (x, y, z) into $(x + \frac{1}{2}, \bar{y} + \frac{1}{2}, z)$. This group has two 1D irreps, Γ_a and Γ_b , with complex OP's $\sigma_a(\mathbf{q})$ and $\sigma_b(\mathbf{q})$. Inversion symmetry I then implies non-trivial relations between the $S_\alpha(\mathbf{q})$'s and the $S_\beta(-\mathbf{q})$'s (which have the same eigenvalue), reducing the number of independent parameters. This should ease future accurate analyses of the neutron data. For Γ_a , symmetry implies

$$m_y \sigma_a = \lambda_a^* \sigma_a, \quad I \sigma_a = e^{i\rho} \sigma_a^*, \quad (2)$$

and similarly for Γ_b (ρ depends on the origin) [19].

For $q_x \neq \frac{1}{2}$, the star of \mathbf{q} contains four wave vectors, namely, $\mathbf{q}_\pm = (q_x, 0, \pm q_z)$ and $-\mathbf{q}_\pm$. Therefore, we introduce two complex OP's, $\sigma_a^+ \equiv \sigma_a(\mathbf{q}_+^{(a)})$ and $\sigma_a^- \equiv \sigma_a(\mathbf{q}_-^{(a)})$, associated with irrep Γ_a and similarly for Γ_b . Then, $F_{M,2} = \sum_{s=a,b} (T - T_{C,s})[|\sigma_s^+|^2 + |\sigma_s^-|^2]$. Rejecting accidental degeneracy, we set $T_{C,a} > T_{C,b}$ and identify the 2DIC phase with our Π_1 phase, associated with a single irrep (the subscript 1 refers to the number of irreps), represented by the σ_a^\pm 's. The transition PM \rightarrow Π_1 occurs at $T = T_{C,a}$, represented by the top (red) surface in Fig. 1. Which OP's actually order depends on the quartic terms in the free energy. For $q_x \neq \frac{1}{2}$, these include

$$F_{M,4}^{(a)} = V_a (|\sigma_a^+|^2 + |\sigma_a^-|^2)^2 + U_a |\sigma_a^+ \sigma_a^-|^2 + \sum_{\mathbf{G}} (W_{aa} [\sigma_a^+ (\sigma_a^-)^*]^2 + cc) \delta[\mathbf{G} - (0, 0, 4q_z)], \quad (3)$$

where \mathbf{G} is a reciprocal lattice vector. For $q_z \neq \frac{1}{4}$ and $T < T_{C,a}$ one has $|\sigma_a^+| = |\sigma_a^-| > 0$ if $U_a < 0$, and only one of the OP's orders otherwise. For q_z near $\frac{1}{4}$, the umklapp term with W_{aa} locks q_z to $\frac{1}{4}$, in a phase called IC₁. Within Landau theory, this happens below a first order surface (blue in Fig. 1), parabolic in J_z .

As T is reduced, more quartic terms need to be considered, notably $W \sum_{m=\pm} \{[\sigma_a(\mathbf{q}_m^{(a)}) \sigma_b(\mathbf{q}_m^{(b)})]^2 + cc\} \delta(\mathbf{q}_m^{(a)} - \mathbf{q}_m^{(b)})$. Assuming that $\mathbf{q}_\pm^{(a)}$ and $\mathbf{q}_\pm^{(b)}$ are almost the same, this term locks the optimal $\mathbf{q}_\pm^{(b)}$ to $\mathbf{q}_\pm^{(a)}$, at some T slightly below $T_{C,a}$, where σ_b has not yet ordered (without involving a phase transition.) Accordingly, we no longer keep the

superscripts (a, b) on the \mathbf{q} 's. As T is further reduced, the tendency of the spins to have fixed length (rather than oscillate sinusoidally) [3,20] may cause a second continuous transition, into the phase Π_2 (or IC₂), where both σ_a and σ_b are nonzero. As shown below, this transition (green surface in Fig. 1) occurs at a temperature which is parabolic in J_x .

We next discuss the special case $q_x = \frac{1}{2}$ (or $J_x = J_{x,c}$, at the back of the 3D diagram in Fig. 1). For $\mathbf{q} = (\frac{1}{2}, 0, q_z)$, the little symmetry group changes: it now contains the additional glide operation m_x [which maps (x, y, z) into $(-x + \frac{1}{2}, y + \frac{1}{2}, z)$]. This group has only one 2D irrep [14,21], with two degenerate complex OP's, σ_1 and σ_2 , and corresponding eigenvectors as listed in Table XVI of Ref. [14] [22]. These OP's transform as [14]

$$m_x \sigma_n = \zeta_n \sigma_n, \quad m_y \sigma_n = \zeta_n \sigma_{3-n}, \quad I \sigma_n = \sigma_{3-n}^*, \quad (4)$$

where $\zeta_n \equiv (-1)^{3-n}$, $n = 1, 2$. Cooling from the PM phase, exactly at $J_x = J_{x,c}$ and $q_z \neq \frac{1}{4}$, one first goes into the CI phase, with the free energy

$$F_M = (T - T_C)[|\sigma_1|^2 + |\sigma_2|^2] + u[|\sigma_1|^2 + |\sigma_2|^2]^2 + W_C |\sigma_1 \sigma_2|^2 + V_C [\sigma_1 \sigma_2^* + \sigma_2 \sigma_1^*]^2. \quad (5)$$

On further cooling, additional umklapp terms cause a first order transition into the CC phase where $\mathbf{q} = (\frac{1}{2}, 0, \frac{1}{4})$. This lock-in happens under a parabola, which connects to the blue parabolas which appear for $q_x \neq \frac{1}{2}$.

We next vary J_x away from $J_{x,c}$. The right-hand side (RHS) of Fig. 1 shows a cut of the 3D phase diagram, at fixed $J_x = J_{x,c} + \Delta J$. For small ΔJ , mirror symmetry, $q_x \rightarrow -q_x$, implies that the inverse susceptibility has two branches of eigenvalues given by $\chi_\pm^{-1}(q_x) \equiv T - T_C + ak_x^2 \pm bk_x \Delta J$, where $k_x = 1/2 - q_x$ and a and b are constants. At quadratic order (i.e., using $F_{M,2}$), this implies that $T_{C,a} - T_{C,b} = 2bk_x^{(0)} \Delta J$, where $k_x^{(0)} = b\Delta J / (2a)$ minimizes $\chi_\pm^{-1}(q_x)$. This gives rise to the (green) $\Pi_1 \rightarrow \Pi_2$ phase boundary, $T_{C,a} - T_{C,b} \propto (\Delta J)^2$.

For q_x close to $\frac{1}{2}$, further cooling may lock it to $\frac{1}{2}$, due to umklapp terms. This may generate transitions into the CI or the CC phase, for T 's below the orange surfaces in Fig. 1. A detailed analysis shows that these surfaces are also parabolic in ΔJ . The actual sequence of transitions then depends on which parabola is narrower. In Fig. 1 we show the case when the green parabolas are broader than the orange ones. In this case, the orange surface represents $\Pi_2 \rightarrow$ CI and IC₂ \rightarrow CC. In the opposite case, the phases Π_2 and IC₂ never appear. As shown in Fig. 1, both parabolas are shifted upwards below the blue surface, where $q_z = \frac{1}{4}$, due to umklapp terms.

Equations (4) and (5) lead to a natural interpretation of neutron scattering results for the CC phase in YMO. Figure 2 shows the Mn³⁺ **a-b** plane spin components in the CC phase of YMO, from the data of Refs. [5] [23] and

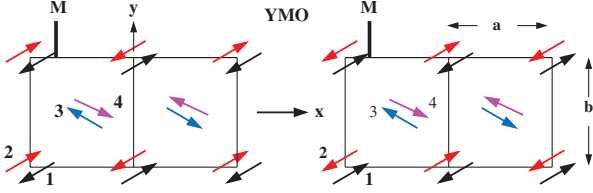


FIG. 2 (color). Schematic diagram of the \mathbf{a} and \mathbf{b} components of the Mn^{3+} spins in a single a - b plane of YMO for the CC phase. The glide m_x consists of a mirror plane M at $x = a/4$ followed by a translation $b/2$ along y . LHS: the structure given in Table III of Ref. [5] (with the \mathbf{c} components not shown). RHS: the structure given in Fig. 2 [38] of Ref. [17] (who reported zero \mathbf{c} components of spin).

[17]. These two structures are obviously similar, and one might ask what symmetry (if any) relates them [24]. Since the structure on the left (right) is even (odd) under the glide operation m_x , we conclude that the structure on the left (right) has $\sigma_2 = 0$ ($\sigma_1 = 0$). Going between these two structures corresponds to a rotation in OP space; the in-plane spin components belong to distinct but equivalent structures. Since either $\sigma_1 = 0$ or $\sigma_2 = 0$, we conclude that in Eq. (5), the net coefficient of $|\sigma_1\sigma_2|^2$ ($W_C - 4|V_C|$ plus the additional umklapp terms) is positive, preventing both OP's from ordering simultaneously [14].

For the phenomenological description of the multiferroicity, the total free energy is $F_{\text{ME}} = F_M + \frac{1}{2}\mathbf{P}^2\epsilon^{-1} + V_{\text{int}}$, where ϵ is the dielectric susceptibility and V_{int} the magnetoelectric (ME) interaction. Although such interactions can also generate a spatially nonuniform \mathbf{P} , here we discuss only the uniform case. We again start with the II and IC phases, where $q_x \neq \frac{1}{2}$. To lowest order, wave vector conservation and time-reversal invariance give [3,25]

$$V_{\text{int}} = \sum_{s,t=a,b} \sum_{\mathbf{q}=\mathbf{q}_{\pm}} \sum_{\gamma} c_{st\gamma} \sigma_s(\mathbf{q}) \sigma_t(-\mathbf{q}) P_{\gamma}. \quad (6)$$

The terms with $s = t$ vanish because they are odd under I . For the II_1 (IC_1) phase, only σ_a is nonzero, and therefore $\mathbf{P} = 0$. To have $\mathbf{P} \neq 0$ with $q_x \neq \frac{1}{2}$ we must have the superposition of two irreps, and this happens only in the II_2 or the IC_2 phases. In these phases, we have

$$V_{\text{int}} = \sum_{\mathbf{q}=\mathbf{q}_{\pm}} \sum_{\gamma} [ir_{\gamma} \sigma_a(\mathbf{q}) \sigma_b(-\mathbf{q}) + cc] P_{\gamma}, \quad (7)$$

and invariance under I requires that r_{γ} is real. From Eq. (2), $\sigma_a \sigma_b^*$ is odd under m_y . For V_{int} to be invariant under m_y , P_{γ} must be odd under m_y : symmetry forces \mathbf{P} to be along $\mathbf{y}(\mathbf{b})$, as observed (Higher order ME interactions weakly violate this result [19]).

In the CC phase, Eq. (6) is invariant under the symmetry operations of Eq. (4) only if [14]

$$V_{\text{int}} = \text{const} [|\sigma_1(\mathbf{q})|^2 - |\sigma_2(\mathbf{q})|^2] P_y. \quad (8)$$

Note that Eqs. (7) and (8) apply whether the *microscopic* ME interactions are due to exchange striction [26] or to

charge ordering [27]. Thus, \mathbf{P} must lie along $\mathbf{y}(\mathbf{b})$ also in the CC phase [28]. Within mean field theory, P_b is proportional to $|\langle \sigma^2 \rangle|$, as is the intensity of the magnetic Bragg peaks. This is confirmed [29] in $\text{RbFe}(\text{MoO}_4)_2$ [which is also described by Eq. (8)] and also apparently for ErMO by Ref. [30] [31]. Since the CC phase is ferroelectric, the fourth order terms in Eq. (5) (plus the umklapp terms) must select $\sigma_1\sigma_2 = 0$, which we deduced from Fig. 2. (The alternative would imply $|\sigma_1| = |\sigma_2|$, hence $\mathbf{P} = 0$.) In fact, the selection of which OP, σ_1 or σ_2 , is nonzero is a result of broken symmetry. An electric field along $\mathbf{y}(\mathbf{b})$ would order P_y , and then Eq. (8) would select either σ_1 or σ_2 , depending on the sign of the field. Therefore we suggest that the sample should be cooled into the FE phase in the presence of a small electric field along y . Depending on the sign of the electric field one should get either the left-hand or the right-hand panel of Fig. 2 [32].

Equation (7) has further implications. First, near the $P \rightarrow \text{II}_1$ transition, a leading fluctuation expansion yields $\Delta\epsilon \propto \langle P_b^2 \rangle \propto |\langle \sigma_a^2 \rangle \langle \sigma_b^2 \rangle|$. Since only σ_a becomes critical there, we expect singularities in ϵ which behave as the energy ($|T - T_{\text{C1}}|^{1-\alpha}$) and (for $T < T_{\text{C1}}$) as the square of the OP ($(T_{\text{C1}} - T)^{2\beta}$), but with $n = 4$ exponents [33]. Indeed, experiments [34] show a break in slope at T_{C1} , apparently confirming this prediction. In addition, this anomaly in the zero frequency dielectric function $\epsilon(\omega = 0)$ reflects the emergence of a resonance in $\epsilon(\omega)$, due to electromagnons [35]. Second, in the II_1 phase $\langle \sigma_a \rangle \neq 0$, so that V_{int} becomes $-2r_b \Im[\langle \sigma_a \rangle \sigma_b^*] P_y$. This bilinear coupling between P_y and $\Im[\langle \sigma_a \rangle \sigma_b^*]$ has several implications on the critical behavior near the $\text{II}_1 \rightarrow \text{II}_2$, should this transition be discovered in some new RMO [36].

Finally, we associate the different RMO's with trajectories on our phase diagram. Since ErMO [6], TmMO [8], and YMO [5] exhibit ferroelectricity in the phase denoted 1DIC, we must identify this phase with our IC_2 phase, where both σ_a and σ_b order. For these materials, the experimental path in parameter space apparently goes from II_1 via IC_2 into the CC phase, as indicated by the dashed lines in the RHS of Fig. 1 (these lines have small slopes, since the experimental optimal \mathbf{q} varies with T : J_x and J_z depend on T due to other degrees of freedom). The last term in Eq. (3) implies that q_z locks to $\frac{1}{4}$ only if both \mathbf{q}_+ and \mathbf{q}_- appear in the IC_1 and IC_2 phases. If $2|W_{aa}| > U_a > 0$, then the two \mathbf{q} 's first appear as the IC_1 phase is entered. If $U_a < 0$, then both wave vectors would have already condensed simultaneously in the II_1 phase. It would be interesting to determine which scenario actually occurs. Since the ME interaction is significant, we suggest to apply an electric field parallel to one of the \mathbf{q} 's, and check whether in the II_1 phase the two \mathbf{q} 's arise in separate domains or coexist within a single domain, following the logic of Ref. [37]. In contrast to the above RMO's, HoMO [9] or TbMO [7] go directly from 2DIC to CM, as along the dotted line in the RHS of Fig. 1. Both sequences are thus allowed by our theory.

The Landau theory is probably less useful at lower T : the low T phases depend on the details of the magnetic interactions, and higher order terms in F_M should be included. Such terms could turn the (orange or blue) surface bounding the CC phase backwards, thus allowing transitions back into the paraelectric II_1 phase, the weakly FE phases II_2 or IC_2 or the FE phase CI. Also, the trajectory describing each material need not be straight (thick dashed line in Fig. 1). A parabolic line, like the thin dashed line, would yield a transition from CC to II_2 (or even to II_1) with decreasing T . In fact, in ErMO [6] the LTI phase seems to have $q_x = \frac{1}{2}$, which identifies this phase with our CI phase. Thus, the observed LTI phase could be any of the phases on the other side of the CC region, paraelectric or weakly ferroelectric. The effects of a magnetic field can be explained as follows: the field generates magnetic moments on the R ion (even above their ordering temperature). Since these ions couple to the Mn ions, their moment results in changes in the effective Mn-Mn interactions, thus changing the “control parameters” and the optimal \mathbf{q} . Apparently, this often moves the material towards the CM regime, resulting in a transition from the low T phase (II_1 or II_2) back into the CC phase [9,11]. Similar effects happen due to pressure [34]. Neutron diffraction measurements in a magnetic field and pressure could help resolve these scenarios.

In summary, we have developed a phase diagram to explain the multiferroic behavior of the family of RMO systems and have proposed several experiments to explore the unusual symmetries of these systems.

We thank M. Kenzelmann, S. H. Lee, and D. Mukamel for helpful interactions. A. A. and O. E. W. acknowledge support from the ISF and from the GIF, and the hospitality of KITP, where this research was supported in part by the National Science Foundation under Grant No. PHY05-51164.

*Also at Tel Aviv University.

- [1] T. Kimura *et al.*, Nature (London) **426**, 55 (2003).
- [2] L. C. Chapon *et al.*, Phys. Rev. Lett. **93**, 177402 (2004).
- [3] G. Lawes *et al.*, Phys. Rev. Lett. **95**, 087205 (2005).
- [4] M. Kenzelmann *et al.*, Phys. Rev. Lett. **95**, 087206 (2005).
- [5] H. Kimura *et al.*, J. Phys. Soc. Jpn. **76**, 074706 (2007).
- [6] S. Kobayashi *et al.*, J. Phys. Soc. Jpn. **73**, 1031 (2004).
- [7] S. Kobayashi *et al.*, J. Phys. Soc. Jpn. **73**, 3439 (2004).
- [8] S. Kobayashi *et al.*, J. Phys. Soc. Jpn. **74**, 468 (2005).
- [9] H. Kimura *et al.*, J. Phys. Soc. Jpn. **75**, 113701 (2006).
- [10] I. Kagomiya *et al.*, Ferroelectrics **286**, 167 (2003).
- [11] D. Higashiyama *et al.*, Phys. Rev. B **72**, 064421 (2005).
- [12] A. P. Cracknell, J. Phys. C **4**, 2488 (1971); D. B. Litvin and W. Opechowski, Physica (Amsterdam) **76**, 538 (1974); Yu. A. Izyumov, V. E. Naish, and R. P. Ozerov, *Neutron Diffraction of Magnetic Materials* (Springer-Verlag, Amsterdam, 1991).
- [13] M. Kenzelmann *et al.*, Phys. Rev. B **74**, 014429 (2006).
- [14] A didactic review of the approach, with more examples, is given by A. B. Harris, Phys. Rev. B **76**, 054447 (2007).
- [15] See also P. G. Radaelli and L. C. Chapon, Phys. Rev. B **76**, 054428 (2007).
- [16] A simple theoretical description of multiferroics [M. Mostovoy, Phys. Rev. Lett. **96**, 067601 (2006); J. J. Betouras *et al.*, Phys. Rev. Lett. **98**, 257602 (2007)] uses a *single* wave vector \mathbf{q} and a *single* vector spin amplitude, $\mathbf{S}(\mathbf{q})$, and constructs combinations of $\mathbf{S}(\mathbf{q})$, $\mathbf{S}(-\mathbf{q})$, \mathbf{q} and \mathbf{P} allowed by symmetry. However, it is not clear how to relate the single $\mathbf{S}(\mathbf{q})$ to the different sublattices within the large unit cell of RMO; see also Ref. [29] and M. Kenzelmann and A. B. Harris, Phys. Rev. Lett. **100**, 089701 (2008).
- [17] L. C. Chapon *et al.*, Phys. Rev. Lett. **96**, 097601 (2006).
- [18] L. D. Landau and I. M. Lifshitz, *Statistical Physics* (Pergamon, New York, 1978), Sec. 139.
- [19] A. B. Harris, M. Kenzelmann, A. Aharony, and O. Entin-Wohlman, arXiv:0803.0945.
- [20] T. A. Kaplan, Phys. Rev. **124**, 329 (1961); T. Nagamiya, in *Solid State Physics*, edited by F. Seitz and D. Turnbull (Academic, New York, 1967), Vol. 20, p. 346.
- [21] G. R. Blake *et al.*, Phys. Rev. B **71**, 214402 (2005).
- [22] See also A. B. Harris, Phys. Rev. B **77**, 019901(E) (2008).
- [23] The wave function found in Ref. [5] (which allowed free variation of all the spins in the unit cell) agrees closely with the eigenvector corresponding to the full group theory predictions, as listed in Table XVI of Ref. [14].
- [24] This degeneracy was also found in a first-principles calculation: C. Wang *et al.*, Phys. Rev. Lett. **99**, 177202 (2007).
- [25] This phenomenological description is similar to that used for simpler commensurate antiferromagnets by S. Goshen *et al.*, Phys. Rev. B **2**, 4679 (1970).
- [26] A. B. Harris, T. Yildirim, A. Aharony, and O. Entin-Wohlman, Phys. Rev. B **73**, 184433 (2006).
- [27] J. van den Brink and D. Khomskii, arXiv:0803.2964.
- [28] In the CC phase, higher order terms, similar to those of I. A. Sergienko *et al.* [Phys. Rev. Lett. **97**, 227204 (2006)], do not come into play here because the quartic terms in Eq. (5) favor either $\sigma_1\sigma_2 = 0$ or $|\sigma_1| = |\sigma_2|$.
- [29] M. Kenzelmann *et al.*, Phys. Rev. Lett. **98**, 267205 (2007).
- [30] Y. Bodenthin *et al.*, Phys. Rev. Lett. **100**, 027201 (2008).
- [31] However, critical fluctuations imply different exponents for P_b and $|\sigma|^2$ [A. Aharony *et al.*, Phys. Rev. Lett. **57**, 1012 (1986)], and this should be checked more carefully.
- [32] A related experiment was recently performed in TbMnO_3 [Y. Yamasaki *et al.*, Phys. Rev. Lett. **98**, 147204 (2007)]. Radaelli also inform us that their unpublished experiments on YMO are consistent with our predictions.
- [33] The isotropic $n = 4$ fixed point is slightly unstable against U_a . For $U_a > 0$ there is probably a crossover to a weak first order transition.
- [34] C. R. dela Cruz *et al.*, Phys. Rev. B **76**, 174106 (2007).
- [35] A. Pimenov *et al.*, Nature Phys. **2**, 97 (2006); A. B. Sushkov *et al.*, Phys. Rev. Lett. **98**, 027202 (2007).
- [36] A. B. Harris, A. Aharony, and O. Entin-Wohlman arXiv:0804.3039.
- [37] S. Skanthakumar *et al.*, Phys. Rev. B **47**, 6173 (1993).
- [38] The labeling of the top and bottom panels in Ref. [17] seems to be switched.